Volume 10 | Number 4 | 28 January 2014 | Pages 533–664

Soft Matter

www.softmatter.org

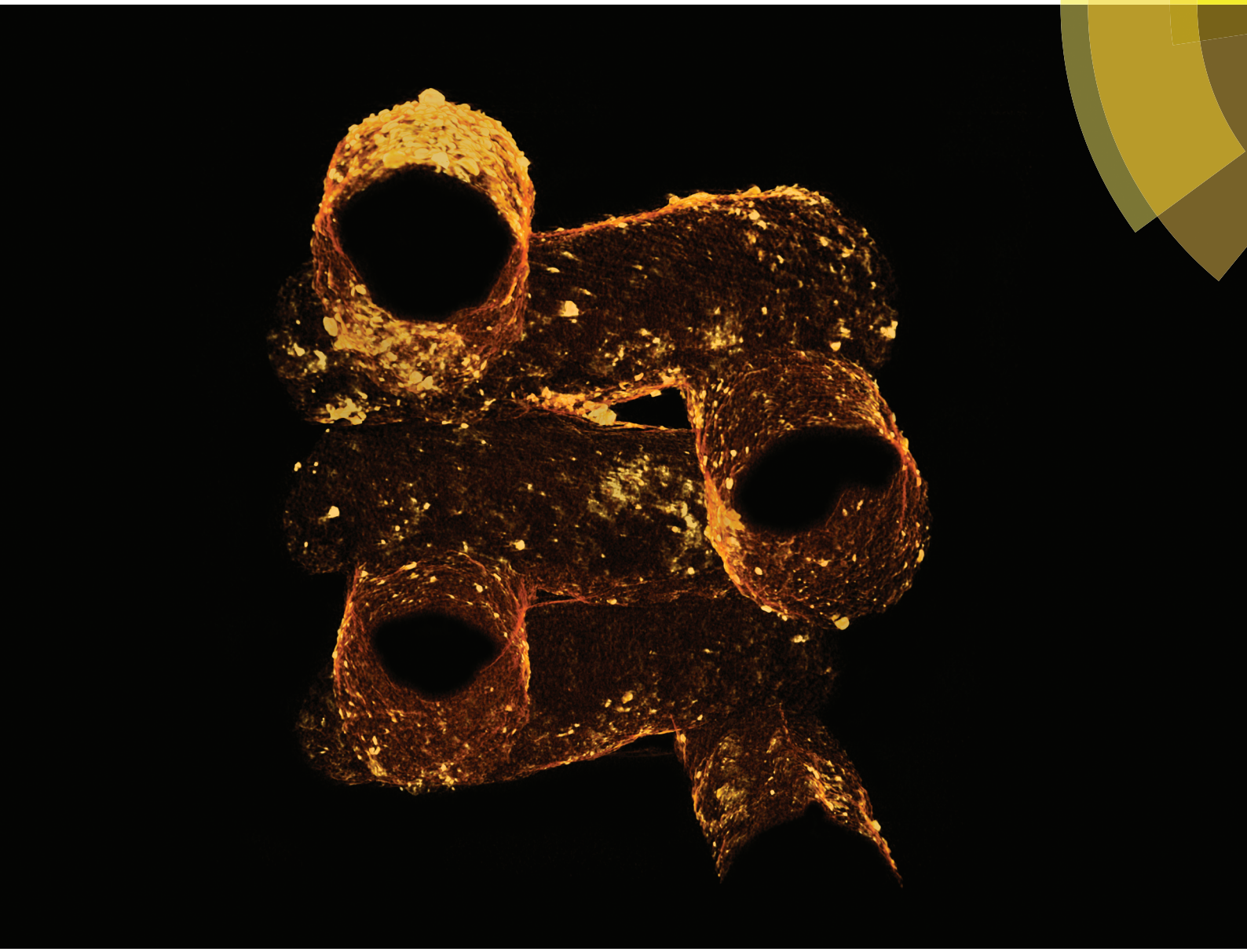

ISSN 1744-683X

ROYAL SOCIETY OF CHEMISTRY

COMMUNICATION

Nancy R. Sottos, Scott R. White *et al.*

Structural reinforcement of microvascular networks using electrostatic layer-by-layer assembly with halloysite nanotubes

Soft Matter

COMMUNICATION

View Article Online
View Journal | View Issue

Cite this: *Soft Matter*, 2014, **10**, 544

Received 29th August 2013
Accepted 25th October 2013

DOI: 10.1039/c3sm52288a

www.rsc.org/softmatter

Structural reinforcement of microvascular networks using electrostatic layer-by-layer assembly with halloysite nanotubes†

Solar C. Olugebefola,[a] Andrew R. Hamilton,[ab] Daniel J. Fairfield,[ac] Nancy R. Sottos*[ac] and Scott R. White*[ad]

We demonstrate a method for tailoring local mechanical properties near channel surfaces of vascular structural polymers in order to achieve high structural performance in microvascular systems. While synthetic vascularized materials have been created by a variety of manufacturing techniques, unreinforced microchannels act as stress concentrators and lead to the initiation of premature failure. Taking inspiration from biological tissues such as dentin and bone, these mechanical deficiencies can be mitigated by complex hierarchical structural features near to channel surfaces. By employing electrostatic layer-by-layer assembly (ELbL) to deposit films containing halloysite nanotubes onto scaffold surfaces followed by matrix infiltration and scaffold removal, we are able to controllably deposit nanoscale reinforcement onto 200 micron diameter channel surface interiors in microvascular networks. High resolution strain measurements on reinforced networks under load verify that the halloysite reduces strain concentrations and improves mechanical performance.

The evolution of two-dimensional microfluidic devices to three dimensions has sparked a growing interest in the use of microchannel networks for structural materials. Polymers and composites containing integrated networks filled with active fluids have demonstrated the ability to indicate internal damage[1–3] as well as to heal from single[4–10] and repeated[11–14] damage events. In this respect, these systems bear a significant resemblance to natural vasculature, which transport fluids throughout biological tissue for various functions including, but not limited to self-healing. We seek to create structures that couple this added functionality with robust structural behavior through the introduction of reinforcing particles at the channel surface.

For self-healing materials the two most documented fabrication methods for creating vascular networks are hollow fiber (HF) embedment or sacrificial scaffolds. The HF approach consists of placing hollow fibers (glass[2,15] or polymer[6]) capable of carrying active fluids into structural composites or foam cores of composite sandwich structures. This method has the advantage of facile incorporation into existing composites manufacturing processes. However, materials with HF are restricted to isolated channels that run uniaxially within each ply in order to align with the surrounding load-bearing fibers. In contrast, sacrificial scaffold networks are formed by the fabrication of an arbitrarily shaped template from a fugitive material that is then surrounded with an epoxy matrix, and removed, leaving a series of interconnected hollow channels.[11–14,16,17] Our research group has studied networks made using direct-write assembly, in which a hydrocarbon microcrystalline wax is extruded to form the scaffold.[18] With appropriate methods of scaffold fabrication, the advantage of this second method is greater control over network design as channels can have non-linear shapes and linkages. More recently, our group has pioneered the use of sacrificial polymers to template vascular features in fiber reinforced composites through heating and vaporization of the sacrificial components (VaSC).[19] Whatever the fabrication approach, the presence of microchannels in a load bearing structural material could reduce structural (mechanical) properties. When subjected to high loads, unreinforced microchannels can act as stress concentrators leading to initiation of premature failure and providing paths for crack propagation.

Within stiffer vascular biological tissues such as dentin (found in teeth) and bone, similar mechanical deficiencies are

[a]*Beckman Institute for Advanced Science and Technology, University of Illinois at Urbana-Champaign, Urbana, IL 61801, USA*

[b]*Mechanical Science and Engineering Department, University of Illinois at Urbana-Champaign, Urbana, IL 61801, USA*

[c]*Materials Science and Engineering Department, University of Illinois at Urbana-Champaign, Urbana, IL 61801, USA. E-mail: n-sottos@illinois.edu*

[d]*Aerospace Engineering Department, University of Illinois at Urbana-Champaign, Urbana, IL 61801, USA. E-mail: swhite@illinois.edu*

† Electronic supplementary information (ESI) available: Experimental details; EDAX spectra of reinforced channels (S1); multilayer thickness as a function of number of layers (S2); microCT reconstruction of a section of microvascular network coated with a nanocomposite multilayer film (S-Movie1); measured and analytically computed strain fields surrounding channels with (PDADMAC/halloysite) films (S3). See DOI: 10.1039/c3sm52288a

mitigated by the presence of complex hierarchical structural features near to channel surfaces. Dentin contains oriented microscale tubules 1–2 μm in diameter running through the length of the tissue. A region of high mineralization and correspondingly high stiffness surrounds each tubule[20] and these regions increase material toughness by forming energy-absorbing microcracks and deflecting larger cracks from their lowest energy paths.[21,22] Haversian canals used to transport nutrients in osteonal bone are another example of biological vasculature in structural materials. These canals are surrounded by a complex lamellar hybrid of hydroxyapatite and collagen fibrils.[23,24] The material architecture results in a stiffness profile that oscillates radially near the canal and functions to arrest impinging cracks[25] and reduce microcrack initiation at canal surfaces.

Tailoring local mechanical properties in a synthetic microvascular material near channel surfaces could potentially enhance the overall mechanical properties of the vascularized material and increase their viability for structural applications. Preliminary research on templates fabricated by robotic deposition of microcrystalline wax[18] suggests that these scaffold-based networks are strengthened by the addition of an alumina microparticle layer to the surface of the scaffold before prepolymer infiltration, thus transferring a reinforcing layer onto the epoxy network channel walls. Fluorescence-based digital image correlation (FDIC) measurements of single channels in cross-section have shown a significant reduction in strain concentrations around surface-modified channels suggesting increased stress tolerance.[26]

FDIC is an extension of the digital image correlation technique and has been used to measure real time, full field strains on the microscale with nanoscale resolution for polymers under load with both surface[26] and interior[27–29] micron-scale inhomogeneities. The technique is ideal for microvascular systems, allowing the direct measurement of the strain field local to embedded channels. Fluorescent silica nanoparticles are first deposited within or onto the surface of a sample to produce a random optical pattern. By imaging the pattern before and during loading, and matching small subsets of images from the initial and deformed states, an optimized correlation coefficient is determined for the local displacement vectors and the displacement gradients within the plane of the image.[30] Regardless of magnification, the technique is accurate to ± 0.1 pixels in displacement as long as a sufficiently distinguishable pattern can be generated.

In order to systematically determine the effects of particle-containing reinforcement layers on the mechanical properties of embedded networks, we use electrostatic layer-by-layer assembly (ELbL) to deposit films containing oxide nanoparticles onto scaffold surfaces before matrix infiltration, leading to embedded-particle regions at the resultant channel surface. We then examine the changes in strain concentration *versus* the increase in reinforcing region thickness for the resultant network. The term layer-by-layer assembly covers a wide range of related techniques for creating nanometer-to-micron thickness films using the sequential exposure of a substrate to solutions containing polymers and/or nanoparticles or other functional components and inducing deposition of those components onto the growing film.[31]

ELbL here more narrowly refers to a well-developed technique for depositing polyelectrolytes and charged particles onto substrates with nanoscale control over layer thickness and chemical composition. Films are built through the alternating immersion of a substrate into aqueous solutions of oppositely charged components leading to incremental buildup of surface films.[32–34] Due to the solution-based nature of the deposition, films can be conformally built onto non-planar substrates, a necessary aspect of modifying three-dimensional scaffolds. The technique is extremely versatile and used to make polymer/polymer, polymer/nanoparticle, and nanoparticle/nanoparticle films. Lvov and coworkers have demonstrated the assembly of halloysite and the polycation poly(diallyldimethyl ammonium) chloride (PDADMAC) onto planar glass substrates with reasonable uniformity.[35] Halloysite is a naturally occurring aluminosilicate nanotube[36] with a net negative surface charge, and is used as a toughening agent in thermoset epoxies.[37–39] Here we seek to use the halloysite/PDADMAC multilayer system to modify the channel structure of scaffold-assembled microvascular network materials by depositing them directly onto network template surfaces and thereby transferring the multilayers to the subsequent matrix.

Adapting halloysite multilayer assembly to fugitive wax scaffolds required overcoming of a number of challenges. To enable ELbL assembly, the standard hydrocarbon-rich fugitive wax ink was modified to carry a negative surface charge through the addition of stearic acid. Inks with too high a proportion of this additive demonstrated unfavorable rheological behavior for scaffold writing. Writable ink formulations contained up to 10 wt% stearic acid, though more ideal writing speeds were possible with ~5 wt%, which was used for almost all sample fabrication. Scaffolds consisting of three stacked, orthogonal layers of parallel 200 μm lines spaced 200 μm apart were written atop substrates – glass slides or silicone molds – used for support during the multilayer deposition process. Flat wax samples on glass slides were also treated in the multilayer deposition process and characterized by scanning electron microscopy (SEM). The ELbL process consists of immersion in a 10^{-2} M aqueous PDADMAC solution followed by water rinsing, then immersion into an aqueous dispersion of 1 g L^{-1} halloysite and further water rinsing. The halloysite was dispersed in solution through ultrasonication and the quality of the dispersion was characterized by dynamic light scattering. The average particle diameter of halloysite in solution was determined to be 153 nm, which suggests single nanotubes without significant quantities of clusters present. Multilayers were assembled by cycling the immersion process repeatedly to yield films denoted by $(\text{PDADMAC/halloysite})_n$ where n is the number of polymer–halloysite bilayers.

An SEM image of a $(\text{PDADMAC/halloysite})_{20}$ film deposited onto a wax surface is shown in Fig. 1a. Nanotubes can be clearly discerned on the surface within the PDADMAC binding polymer, completely covering the underlying wax surface. Electron dispersive X-ray spectroscopy confirmed the presence of

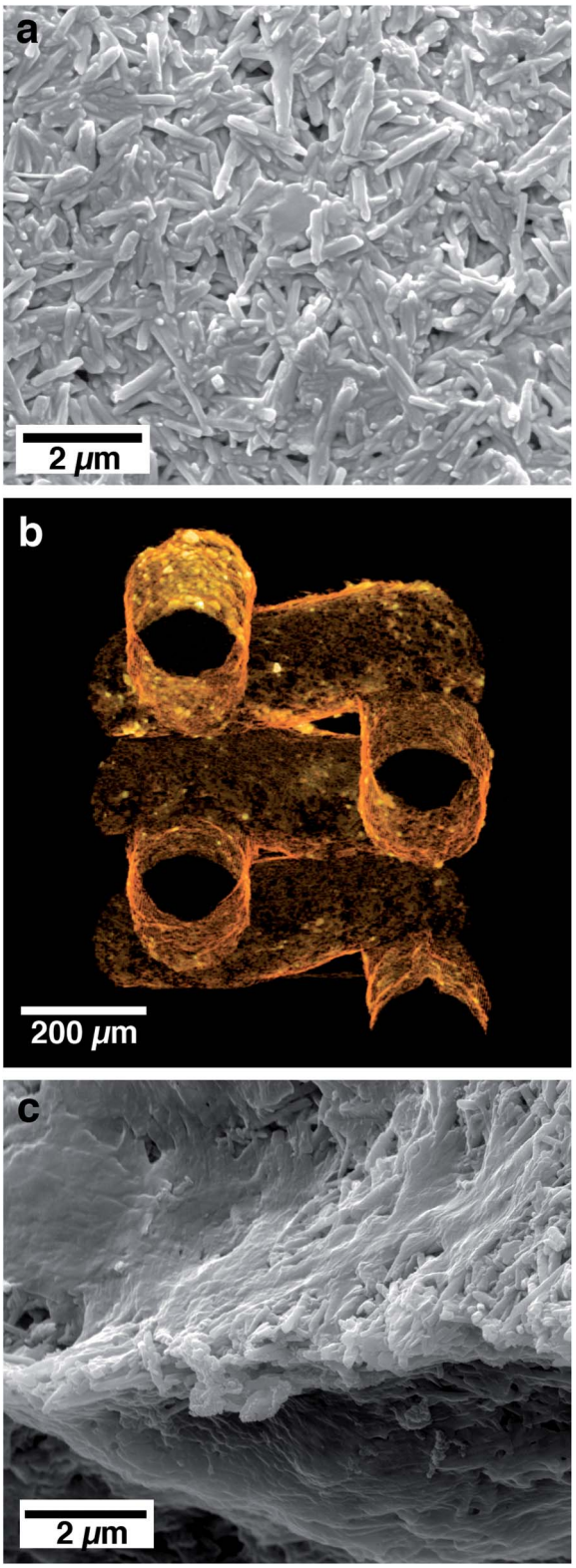

Fig. 1 (a) SEM image of PDADMAC/halloysite multilayer deposited onto flat wax surface showing isotropic nanotube orientation. (b) MicroCT reconstruction of $(PDADMAC/halloysite)_{80}$ multilayer deposited onto fugitive network scaffold. Multilayer coverage reaches all locations on the scaffold surface. (c) SEM image of epoxy matrix with embedded PDADMAC/halloysite multilayer at the intersection between two channels. The minimum radius of curvature for the deposited halloysite is less than 2 μm.

aluminum, silicon, oxygen and carbon consistent with the presences of halloysite, wax and polymer (see ESI†). In order to assess the overall coverage of the multilayer film on fabricated scaffolds, we imaged samples with microscale computed X-ray tomography (MicroCT). Fig. 1b shows a representative 3-dimensional reconstruction of a scaffold section with a deposited 80 bilayer film, in which the brightness correlates to X-ray contrast. The film demonstrably reaches all locations on the scaffold, including high curvature regions where the extruded wax lines intersect. The voxel resolution of the instrument is limited to approximately 1 μm^2 when examining a full network and thinner layer regions manifest as gaps in the high contrast coating while thicker regions appear as bright spots.

After multilayer assembly, scaffolds were surface functionalized with a glycidyl silane to promote epoxy adhesion then infiltrated with a liquid epoxy prepolymer and cured. Scaffolds were removed by a combination of heating and chemical solvation leaving hollow channels within the matrix. To determine the efficacy of transfer of the multilayer to the epoxy surface, fractured network specimens were examined at channel intersections. An SEM image of a representative junction between two channels shows the narrowing edge of epoxy before they meet in Fig. 1c. The presence of halloysite is evident to a gap size of approximately 1–2 μm demonstrating the conformal nature of the deposition. Due to the fragility of the scaffold, measuring multilayer thickness directly from deposition was infeasible. Instead, we fabricated single channel samples and then fractured them to reveal axial cross-sections. Fig. 2 shows channel edges of samples with increasing numbers of bilayers embedded in the epoxy matrix. The lack of visible interface between the epoxy and the multilayers is evidence of favorable bonding. From these images, the thickness is correlated to the number of bilayers deposited (see ESI†). As suggested by the MicroCT measurements of the scaffold, the thickness variation increases significantly with the number of bilayers (see ESI†). The multilayer assembly process exhibits linear thickness growth with a per-bilayer thickness of approximately 188 nm, which is only slightly larger than the average halloysite tubule diameter measured by light scattering (153 nm). This value suggests monolayer or near-monolayer deposition per cycle. The variation in multilayer thickness is evident from MicroCT scans of an 80-bilayer reinforced network after scaffold removal (ESI†).

To determine the effects of increasing layer thickness on mechanical properties, we performed FDIC measurements on samples with single channels under uniaxial tension normal to the channel axis. Images taken before and during loading were correlated to yield a displacement field along with corresponding displacement gradient fields. To act as a control, far-field strains were first measured in flat regions of each sample free of surface features, and strain uniformity was confirmed by a standard deviation over the image field of less than 5 percent. Fig. 3a shows the normalized ε_{xx} strain fields near the channel for both unreinforced and with (PDADMAC/halloysite) multilayers embedded. In these images, the loading direction is horizontal and the maximum strains are located directly above and below the channels while the minimum strains are located along the

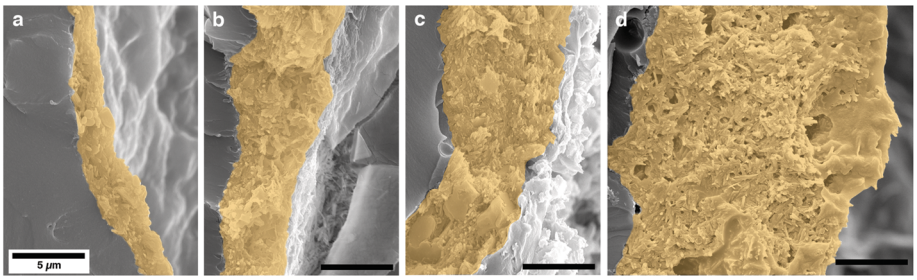

Fig. 2 SEM imaged microvascular channel longitudinal cross-sections showing matrix-embedded PDADMAC/halloysite reinforcement at a) 10-bilayers, b) 20-bilayers, c) 40-bilayers and d) 80-bilayers. Images are false colored to distinguish multilayers from bulk epoxy.

loading axis. Compared to the control sample the presence of the multilayer suppresses the amplitude of these maximum strains. The effect of 20-bilayers is less pronounced than that for 40- and 80-bilayers. In the latter cases the strain along the vertical axis eventually drops below that of the far-field strain further from the channel ($\varepsilon_{xx} < 1$) suggesting a significant reinforcing effect. A histogram of strain values in the regions above and below the whole channel clearly illustrates the decrease in strain with increasing halloysite layer thickness (Fig. 3b). At 80-bilayers, the mode of the strain field – taken as the peak of the histogram – transitions below that of the far-field strain, though there is still an observable strain concentration near the channel edge.

In order to estimate the elastic modulus of the reinforcing material, we compared strain fields for 80-bilayer samples to analytical solutions for channels with a reinforced interlayer ring in an infinite plate.[40] The multilayer thickness measured by SEM and channel diameter measured by optical imaging were used as inputs for the analysis. Theoretical predictions reasonably matched the FDIC strain field when the ring modulus was estimated to be 10 GPa. Using this modulus value to simulate strain fields for 40- and 20-bilayer samples also matched experimental results (ESI†). This value is significantly lower than bulk values for alumina or silica, and more than an order of magnitude lower than theoretically predicted values for single halloysite nanotubes, which are in the range of 234–339 GPa.[41] The reduced modulus is likely due to two factors. The first is weak bonding between the halloysite and the PDADMAC within the multilayer, which is ionic rather than covalent. Secondly, the introduction of halloysite particles to bulk epoxy has been shown to significantly increase toughness, but the effects on modulus have been less pronounced.[36,38] Ideally, strengthening the reinforcement layer would involve promoting stronger bonds between the polymer and the nanoparticles[42] and increasing the relative ratio of oxide to polymer. Both of these effects may be achieved by increasing the particle size, or by changing the polymer and particle charge densities in solution to control the degree of deposition of each component per layer.

In summary, the electrostatic layer-by-layer assembly technique can be used to incorporate halloysite nanotube reinforcement at channel surfaces in microvascular networks. The deposition is facile for reasonably complex microscale features, limited by the size of the deposition particles. Halloysite acts as a local reinforcement at appropriate thicknesses and bonds readily to epoxy matrix materials. By reducing the stress concentration near microchannels, the multilayer reinforcement should improve the matrix mechanical properties and therefore the structural capacity. The ELbL technique should be applicable to deposition of other types of oxide nano- and microparticles, which may demonstrate even stronger reinforcing effects depending on particle shape and size.

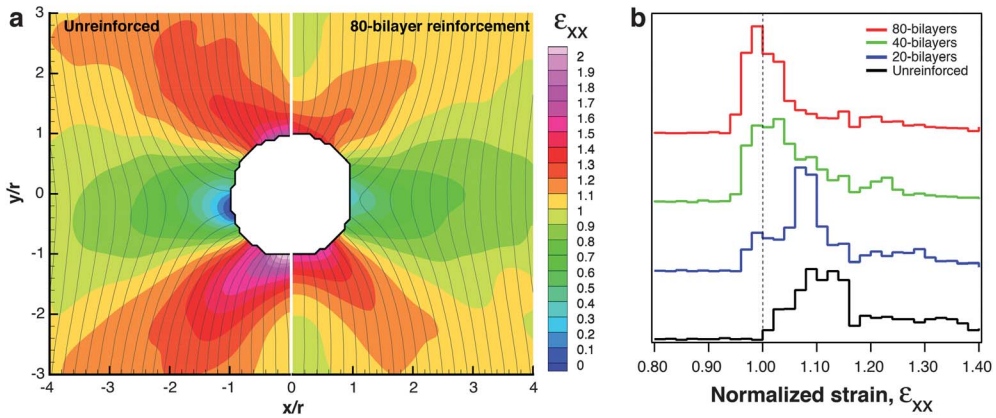

Fig. 3 a) Normalized strain field as measured by FDIC for an unreinforced (left) and an 80-bilayer PDADMAC/halloysite multilayer-reinforced (right) microvascular channel. b) Histograms of strain measured above and below sample microchannels along $x/r = 0$ indicating a reduction in strain for increasing multilayer thickness.

Acknowledgements

This work was supported by the Air Force Office of Scientific Research Multidisciplinary University Research Initiative (grant F49550-05-1-0346). We are grateful to the Imaging Technology Group at the Beckman Institute for their imaging expertise and use of their facilities.

Notes and references

1 S. M. Bleay, C. B. Loader, V. J. Hawyes, L. Humberstone and P. T. Curtis, *Composites, Part A*, 2001, **32**, 1767.
2 J. W. C. Pang and I. P. Bond, *Composites, Part A*, 2005, **36**, 183.
3 J. W. C. Pang and I. P. Bond, *Compos. Sci. Technol.*, 2005, **65**, 1791.
4 R. S. Trask and I. P. Bond, *Smart Mater. Struct.*, 2006, **15**, 704.
5 R. S. Trask, G. J. Williams and I. P. Bond, *J. R. Soc., Interface*, 2007, **4**, 363.
6 H. R. Williams, R. S. Trask and I. P. Bond, *Smart Mater. Struct.*, 2007, **16**, 1198.
7 H. R. Williams, R. S. Trask and I. P. Bond, *Compos. Sci. Technol.*, 2008, **68**, 3171.
8 G. J. Williams, I. P. Bond and R. S. Trask, *Composites, Part A*, 2009, **40**, 1399.
9 C. J. Norris, G. J. Meadway, M. J. O'Sullivan, I. P. Bond and R. S. Trask, *Adv. Funct. Mater.*, 2011, **21**, 3624.
10 C. J. Norris, J. A. P. White, G. McCombe, P. Chatterjee, I. P. Bond and R. S. Trask, *Smart Mater. Struct.*, 2012, **21**, 094027.
11 K. S. Toohey, N. R. Sottos, J. A. Lewis, J. S. Moore and S. R. White, *Nat. Mater.*, 2007, **6**, 581.
12 K. S. Toohey, C. J. Hansen, J. A. Lewis, S. R. White and N. R. Sottos, *Adv. Funct. Mater.*, 2009, **19**, 1399.
13 C. J. Hansen, W. Wu, K. S. Toohey, N. R. Sottos, S. R. White and J. A. Lewis, *Adv. Mater.*, 2009, **21**, 4143.
14 A. R. Hamilton, N. R. Sottos and S. R. White, *Adv. Mater.*, 2010, **22**, 5159.
15 A. Kousourakis, A. P. Mouritz and M. K. Bannister, *Compos. Struct.*, 2006, **75**, 610.
16 R. S. Trask and I. P. Bond, *J. R. Soc., Interface*, 2010, **7**, 921.
17 L. M. Bellan, S. P. Singh, P. W. Henderson, T. J. Porri, H. G. Craighead and J. A. Spector, *Soft Matter*, 2009, **5**, 1354.
18 D. Therriault, S. R. White and J. A. Lewis, *Nat. Mater.*, 2003, **2**, 265.
19 A. P. Esser-Kahn, P. R. Thakre, H. Dong, J. F. Patrick, V. K. Vlasko-Vlasov, N. R. Sottos, J. S. Moore and S. R. White, *Adv. Mater.*, 2011, **23**, 3654.
20 G. Balooch, G. W. Marshall, S. J. Marshall, O. L. Warren, S. A. S. Asif and M. Balooch, *J. Biomech.*, 2004, **37**, 1223.
21 R. K. Nalla, J. H. Kinney and R. O. Ritchie, *J. Biomed. Mater. Res., Part A*, 2003, **67**, 484.
22 R. K. Nalla, J. H. Kinney and R. O. Ritchie, *Biomaterials*, 2003, **24**, 3955.
23 J. Black, R. Mattson and E. Korostoff, *J. Biomed. Mater. Res.*, 1974, **8**, 299.
24 F. G. Evans and R. Vincentelli, *J. Biomech.*, 1974, **7**, 1.
25 H. S. Gupta, U. Stachewicz, W. Wagermaier, P. Roschger, H. D. Wagner and P. Fratzl, *J. Mater. Res.*, 2006, **21**, 1913.
26 A. R. Hamilton, N. R. Sottos and S. R. White, *Exp. Mech.*, 2010, **50**, 255.
27 T. A. Berfield, J. K. Patel, R. G. Shimmin, P. V. Braun, J. Lambros and N. R. Sottos, *Small*, 2006, **2**, 631.
28 C. Franck, S. Hong, G. Ravichandran, S. A. Maskarinec and D. A. Tirrell, *Exp. Mech.*, 2007, **47**, 427.
29 B. Samuel, M. Demirel and A. Haque, *J. Micromech. Microeng.*, 2007, **17**, 2324.
30 H. A. Bruck, S. R. McNeill, M. A. Sutton and W. H. Peters, *Exp. Mech.*, 1989, **29**, 261.
31 G. Decher and J. B. Schlenoff, *Multilayer Thin Films*, Wiley-VCH, 2003.
32 G. Decher and J. D. Hong, *Makromol. Chem., Macromol. Symp.*, 1991, 321.
33 Z. Tang, Y. Wang, P. Podsiadlo and N. A. Kotov, *Adv. Mater.*, 2006, **18**, 3203.
34 G. Decher, in *Multilayer Thin Films: Sequential Assembly of Nanocomposite Materials*, ed. G. Decher and J. B. Schlenoff, Wiley-VCH, Weinheim, Germany, 2003, vol. 1, pp. 1–46.
35 Y. Lvov, R. Price, B. Gaber and I. Ichinose, *Colloids Surf., A*, 2002, **198**, 375.
36 E. Joussein, S. Petit, J. Churchman, B. Theng, D. Righi and B. Delvaux, *Clay Miner.*, 2005, **40**, 383.
37 M. Liu, B. Guo, M. Du, X. Cai and D. Jia, *Nanotechnology*, 2007, **18**, 455703.
38 Y. Ye, H. Chen, J. Wu and L. Ye, *Polymer*, 2007, **48**, 6426.
39 S. Deng, J. Zhang, L. Ye and J. Wu, *Polymer*, 2008, **49**, 5119.
40 G. N. Savin, *Stress distribution around holes*, NASA, Springfield, VA, 1970, p. 997.
41 L. Guimaraes, A. N. Enyashin, G. Seifert and H. A. Duarte, *J. Phys. Chem. C*, 2010, **114**, 11358.
42 P. Podsiadlo, A. K. Kaushik, E. M. Arruda, A. M. Waas, B. S. Shim, J. Xu, H. Nandivada, B. G. Pumplin, J. Lahann, A. Ramamoorthy and N. A. Kotov, *Science*, 2007, **318**, 80.

